PROOF COPY 006212JAP

Composition fluctuation in InGaN quantum wells made from molecular beam or metalorganic vapor phase epitaxial layers

P. Ruterana[a)]
ESCTM-CRISMAT, 6 Bd Maréchal Juin, 14050 Caen Cedex, France

S. Kret
ESCTM-CRISMAT, 6 Bd Maréchal Juin, 14050 Caen Cedex, France and Institute of Physics, PAS, Al. Lotników 32/46, 02-668 Warszawa, Poland

A. Vivet
Laboratoire Universitaire de Recherche Scientifique d'Alençon, Institut Universitaire de Technologie, 61250 Damilly, France

G. Maciejewski and P. Dluzewski
Instytut Podstawowych, Problemów Techniki PAN, Ul.Świętokrzyska 21, Warszawa, Poland

(Received 19 November 2001; accepted for publication 6 March 2002)

Using strain analysis on high resolution electron microscopy images and finite element modeling of InGaN quantum wells (QWs), it is shown that the In composition changes inside the layers can be accurately determined. The analyzed samples were nominally grown with 15%–17% In composition by molecular beam or metalorganic vapor phase epitaxy. Inside these QWs, the In composition is not homogeneous. Finite element modeling strongly suggests that the measured strain corresponds most probably to InN clusters whose size depends on the growth method. © *2002 American Institute of Physics.* [DOI: 10.1063/1.1473666]

PROOF COPY 006212JAP

I. INTRODUCTION

The last ten years have brought about a large development of blue light emitting diodes and laser diodes made in GaN based multilayers,[1] the active region of these devices is made of InGaN/GaN quantum wells (QWs). Their high luminescence in comparison to GaAs based devices is in contrast with the huge densities of defects present inside the layers (10^{8-10} cm^{-2}). The first observations attributed this performance to the presence of In rich nanometer islands, which behave like quantum dots.[2] This was in agreement with theoretical calculations, which predicted that InN and GaN are not miscible for typical growth temperatures around 800 °C.[3] Subsequently, a number of experimental reports have shown that phase separation occurs during growth[4] or annealing of InGaN layers.[5] These results appear to agree with the optical measurements, which showed strong localization effects that exist even for very low In content.[6] In as low as 1%–2% In quantum wells, such studies indicate that the high luminescence can be attributed to InN nano-clusters whose size may increase with subsequent In concentrations.[7,8] In parallel, a number of other behaviors have been reported for InGaN alloys such as the incorporation of In up to $x=0.8$ in GaN/$In_xGa_{1-x}N$/GaN double heterostructures or multiple types of ordering along the [0001] direction.[9–11] These reports suggest that the InGaN system is complex and that the nature of the high efficiency emitter in this system may not yet have been completely identified. To this end, high-resolution electron microscopy (HREM) can be used to investigate the structure at nanometer scale. Using pattern recognition on cross-section HREM images taken in $[11\bar{2}0]$ zone axis, Kisielowski, Liliental Weber, and Nakamura[12] have shown that In segregates in 1–3 nm areas inside GaN/$In_xGa_{1-x}N$/GaN heterostructures. More recently, Gerthsen *et al.*[13] analyzed lattice fringe images obtained close to $[10\bar{1}0]$ zone axis; they pointed out that the In may be present in clusters of 3–5 nm lateral size with concentration up to 70%–80% inside layers of 10%–20% nominal composition.

In the following, we present a comparative study of metalorganic chemical vapor deposition (MOCVD) and molecular beam epitaxy (MBE) InGaN quantum wells grown with similar nominal In composition (15%–17%). By a combination of finite element analysis and strain measurements, it has been possible to show that in both types of samples, composition fluctuations of In take place. Scaling the strains in homogeneous composition by finite element analysis, it is shown that, for MOCVD samples, the clusters are slightly larger and well separated with an In composition close to 40% inside the clusters. In the MBE layers, highest strains (>0.05) are measured in the middle of the QWs, but the In fluctuations are shown to take place at a smaller scale. A detailed finite element analysis of the possible three-dimensional structure of indium distribution allows to conclude that, in both types of samples, clustering into pure InN cannot be excluded.

II. EXPERIMENTAL PROCEDURE

The investigated ternary layers were $In_xGa_{1-x}N$ QWs MBE or MOCVD with a nominal composition of 15%–17%

a)Author to whom correspondence should be addressed; electronic mail: ruterana@ismra.fr

PROOF COPY 006212JAP

PROOF COPY 006212JAP

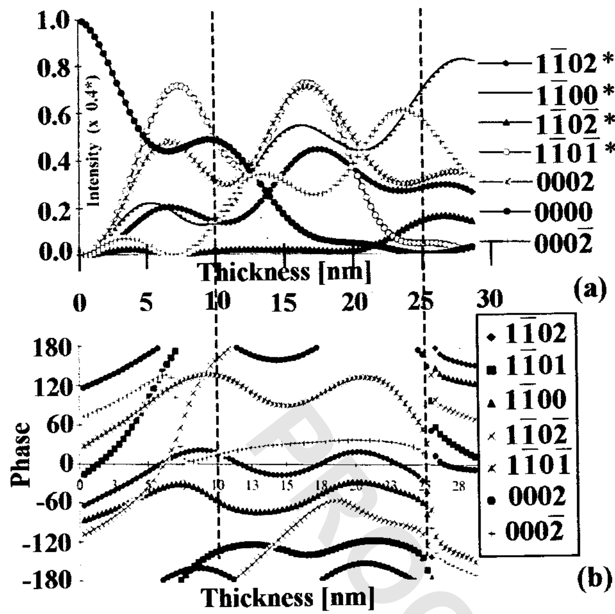

FIG. 1. Beam profiles for GaN along the $[11\bar{2}0]$ zone axis. (a) Intensity, (b) phases are relative to the 0000 beam.

In. The nominal thickness was 4.5 nm for the MBE multi quantum wells and 2.4 nm for a set of three MOCVD quantum wells.

The cross-section transmission electron microscopy (TEM) samples were prepared along the $[11\bar{2}0]$ zone axis. They were mechanically polished down to 100 μm and then dimpled to 10 μm. For electron transparency, ion milling was used at 5 kV and 15° incidence, with the sample holder kept at liquid nitrogen in order to minimize the ion beam damage; it has been known for a long time that In containing materials are beam sensitive.[14] High-resolution transmission electron microscopy (HRTEM) was carried out on a Topcon 002B microscope operating at 200 KV with point resolution of 0.18 nm.

III. APPROACH TO THE LOCAL IN COMPOSITION DETERMINATION

As the lattice parameter of InN is larger than that of GaN, the layers are grown in pseudomorphic regime below the critical thickness, therefore the lattice parameter a_{InGaN} is strained to equal a_{GaN}, and the c_{InGaN} is expanded depending on the In composition and elastic constants. This distortion along the growth direction can be precisely extracted from HREM micrographs by image processing.

For this analysis, the HREM observations were carried out along the $[11\bar{2}0]$ GaN zone axis and 0001, 0002, 0004, $10\bar{1}1$, and $1\bar{1}02$ beams were used to form the images. As can be seen on the intensity and phase profiles (Fig. 1) of GaN, unlike AlN in which the weak phase object approximation holds until more than 10 nm thickness,[15] the image contrast is very sensitive to variation of foil thickness. There is a first maximum of the diffracted beams close to 5 nm, then, until 12 nm, the 000 beam almost keeps the same intensity, whereas that of the other beams decreases [Fig. 1(a)]. Above 15 nm, the intensity of the transmitted beam drops strongly. As will be shown on the experimental images, these features can be used to estimate the sample thickness and this was found to be useful in modeling the strain fields.

Images were recorded on negative films and digitized by sampling of 36 pixel/nm and 8 bits dynamics. Processed images had typically 2048×2048 or 4096×2048 pixel size; the analyzed areas were about 60×60 nm. Analysis of images of large crystal areas helps us to visualize the long-range thickness variation; thus we are able to chose areas of homogeneous contrast and thickness below 10 nm for analysis. The thickness (t) estimation was based on the position of observed zone in relation with the thickness fringes which are known with an accuracy of $\Delta t = 5$ nm.

Processing of experimental images was performed using routines written in analytical language for images of Optimas graphical environment.[16] For noise reduction, we used Wiener filtering and localization of intensity maxima by 4 parabolas as described by Rosenauer *et al.*[17] The reference lattice with unit cell $d(0002)*d(10\bar{1}0)$ was determined in GaN area and extrapolated to the quantum well region. Next, the discreet displacement field component $u_x(x,z)$ parallel to the growth direction **x** was calculated as the difference between the corresponding reference and deformed lattice nodes d_{ij}. The lattice distortion components parallel to the growth direction were obtained as the derivatives $\epsilon_{xx} = \partial u_x/\partial x$ as described in Ref. 18. In a bulk multilayer sample, ϵ_{xx} can be related to local In composition within the Vegard law approximation

$$c_{\mathrm{In}_x\mathrm{Ga}_{1-x}\mathrm{N}} = c_{\mathrm{GaN}} + x_{\mathrm{In}}(c_{\mathrm{InN}} - c_{\mathrm{GaN}})$$

$$c_{\mathrm{In}_x\mathrm{Ga}_{1-x}\mathrm{N}} = c_{\mathrm{GaN}}(1+\epsilon_{xx}), \tag{1}$$

where $c_{\mathrm{GaN}} = 0.5185$ nm, $c_{\mathrm{InN}} = 0.527$ nm.

In a TEM cross-section thin foil of pseudomorphic multilayers, the lattice parameters of the individual layers depend on GaN/InGaN thickness ratio, elastic constants, foil normal, and the foil thickness.

In recent similar studies[13] only the two limits of the thin foil and bulk sample approximations were used to calculate the error bars for composition evaluation. We can reduce this error by modeling the real sample geometry. In a typical experiment geometry, the surface normal (y direction) and the electron beam are parallel to the $[11\bar{2}0]$ zone axis, the growth direction x is parallel to [0001]. The TEM thin foil prepared for cross section observation undergoes partial strain relaxation: the pseudomorphically strained InGaN layer relaxes in the y direction; the strain and stress state are modified as compared to the bulk material. The surface of the thin foil and the lattice planes are curved. For these GaN and InGaN layers, the deformation is not pseudomorphic: the lattice parameters of GaN layer are expanded in the y direction and shortened in the x direction, therefore the measured expansion of the lattice parameters of InGaN is smaller than before thinning. This type of thin foil relaxation was previously investigated by Treacy and Gibson[19] for a GaAs/GaInAs superlattice and [001] foil normal using Fourier series methods. In their finite element study of InGaAs, Tillmann, Lentzen, and Rosenfeld[20] used the lattice mis-

PROOF COPY 006212JAP

PROOF COPY 006212JAP

match and the thermal expansion coefficients to induce the strain, and, by heating the heterostructure with steps of 1 K, they generated the desired configuration.

In the present approach, we calculate the strain distribution in an xy section of the TEM sample, a projection along the y direction leads to averaged profiles of the strain which are directly comparable to the data extracted from experimental HREM images.[13] This two-dimensional (2D) finite element (FE) calculation uses a Taylor's FEAP program,[21] which was modified to take into account the finite deformation.[22] The formalism of the finite deformation (where the calculation distinguishes precisely the initial and final configurations) is suitable for a proper description of highly strained heterostructures in which a deformation of several percent takes place. Due to the high deformation levels, an important role is played by the elastic nonlinearity; we applied the anisotropic hyperelastic model that uses hardening for the compression and softening for the extension.[23] This asymmetry in the behavior of the material corresponds to experimental observations and to atomistic simulations based on interatomic potentials.[24] Our numerical procedure allows us to impose stress free lattice deformation at each node. This initial deformation was calculated using the relationship between lattice parameters of the relaxed materials. For nodes corresponding to GaN, $\epsilon_{xx}=0$ and $\epsilon_{yy}=0$, whereas for InGaN nodes, the following deformation was attributed:

$$\epsilon_{xx}=(c_{\mathrm{InGaN}}-c_{\mathrm{GaN}})/c_{\mathrm{GaN}}$$

and

$$\epsilon_{yy}=(a_{\mathrm{InGaN}}-a_{\mathrm{GaN}})/a_{\mathrm{GaN}}.$$

The calculation is carried out in the xy plane; however, it is necessary to take into account additional deformations along the z direction. In this direction, the lattice of the GaN and InGaN are coherent with common lattice parameter a_z, which depends on the layers' relative thickness (geometry), chemical composition and elastic constants. We consider that in a relaxed sample, the volume is close to that of the corresponding bulk with the same number of unit cells. So, the additional equilibrium equation for stresses in the z direction is introduced into the algorithm to obtain a realistic value of the a_z: $\int_S \sigma_{zz}(x,y)=0$ (S denotes the area of xy cross section of the sample). The final position of the nodes is calculated using a newly developed element in the FEAP program and the Newton–Raphson method was used to solve the equilibrium equations. This nine-node biquadratic element for planar stress calculation uses logarithmic stress–strain relation in this case of anisotropic hexagonal materials.[25]

All calculations were performed for abrupt interfaces between the GaN and $In_xGa_{1-x}N$ layers. We have investigated two types of geometries: (i) $G1$ ($L1=10$ nm of GaN, $L2=5$ nm of InGaN), foil thickness ($t=1-50$ nm) and composition ($x=0.05-0.6$). (ii) For the MOCVD sample, the geometry $G2$ was used: the thick layer of GaN ($L0=50$ nm) is followed by three layers of InGaN ($L1=4$ nm) separated by a GaN spacer $L2=8$ nm and $L3=10$ nm thick cap layer. This geometry corresponds exactly to experimental configuration of the studied epilayers. The elastic constants for different indium composition were calculated using the Vegard's law on the values of InN and GaN (Table I).

TABLE I. Lattice parameters and elastic constants used for calculation after Ref. 26.

	GaN	InN
a (Å)	5.185	5.72
c (Å)	3.189	3.52
$c11$ (GPa)	374.20	223.00
$c12$	141.40	115.00
$c13$	98.10	92.00
$c33$	388.60	224.00
$c44$	98.30	48.00

From FE calculation, the 2D distortion distribution is extracted and Fig. 2(a) shows the contour maps of ϵ_{xx} component in the xy plane obtained for a foil thickness $t=10$ nm. For a direct comparison with HREM images, averaging of ϵ_{xx} was performed. In these one-dimensional profiles [Fig. 2(b)], it can be seen that the deformation occurs in InGaN as well as in GaN layers. This expansion results in a contraction in the x direction which can be seen in Fig. 2(b) where the $\epsilon_{xx}(x)$ values are negative close to the interface. In

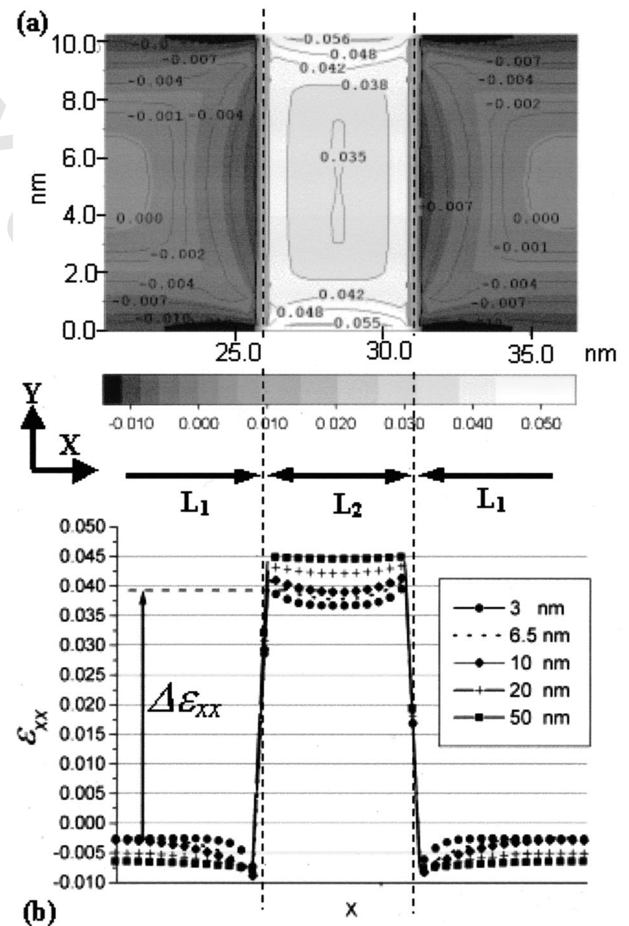

FIG. 2. (a) Calculated $\epsilon_{xx}(x,y)$ distribution after stress relaxation for In concentration %In=30, $t=10$ nm, $L1=10$ nm, $L2=20$ nm. (b) Profiles of $\epsilon_{xx}(x)$ obtained by averaging of $\epsilon_{xx}(x,y)$ along the y direction for 30% of indium concentration and $t=5$, 10, 15, 30 nm. All values are expressed with the relaxed GaN lattice as reference.

PROOF COPY 006212JAP

PROOF COPY 006212JAP

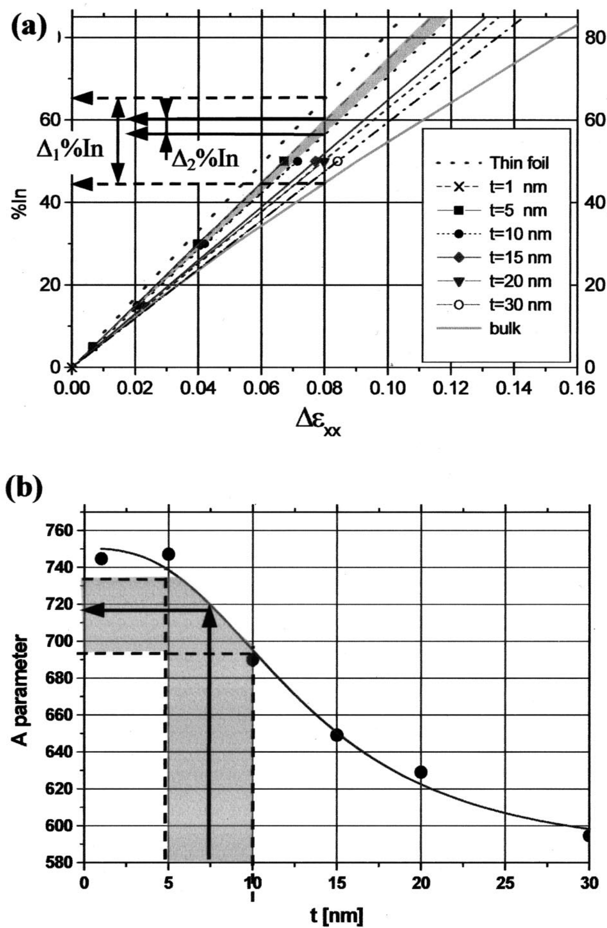

FIG. 3. (a) $\Delta\epsilon_{xx}$ vs In composition for layer different geometries. (b) **A** parameter ($x_{\mathrm{In}}=\mathbf{A}\Delta\epsilon_{xx}$) in function of foil thickness.

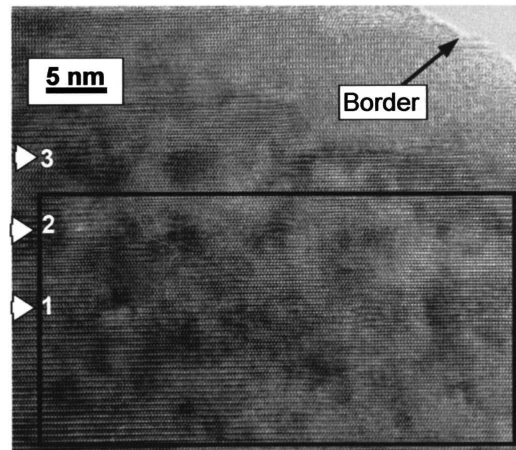

FIG. 4. HRTEM image of three InGaN (MOCVD) QWs along the $[11\bar{2}0]$ zone axis. The black frame shows the composition evaluation area.

the FE calculations, the perfect GaN lattice is taken as the reference. On HREM images of QWs, the deformed GaN lattice near the ternary layer is used as the reference, and the measured distortion in $In_xGa_{1-x}N$ layer corresponds to $\Delta\epsilon_{xx}$ shown by arrow in Fig. 2(b). The next step is to calculate a set of $\Delta\epsilon_{xx}$ for different foil thickness and In concentration in the ternary layer and compare them to experimentally measured $\Delta\epsilon_{xx}^{\mathrm{exp}}$. In this way, the composition can be determined. For example, the calculated $\Delta\epsilon_{xx}$ values for different thickness and composition for geometry $G1$ are drawn in Fig. 3(a). As we can see, for a given foil thickness, the indium concentration is linear in function of $\Delta\epsilon_{xx}$ and can be expressed as: $x_{\mathrm{In}}=\mathbf{A}_{G1}\Delta\epsilon_{xx}$. **A** depends on the foil thickness t as shown in Fig. 3(b). The error bars on composition evaluation depend mainly on the accuracy in foil thickness determination. For example, for a foil thickness between 5 and 10 nm, and a measured $\Delta\epsilon_{xx}$ is 0.08, the indium concentration x of $In_xGa_{1-x}N$ is 55%–60% [as shown by arrows in Fig. 3(a)].

This is a substantial improvement to using the thin/bulk limits, where the error bar is Δ_1% In=20 (44%–65% as shown by dashed arrows). From Fig. 3(b), the most favorable range of foil thickness is between 0 and 5 nm and above the 20 nm where the variation of A versus t is slow.

Similar scaling curves can be obtained for geometry $G2$, which correspond to the MOCVD sample. In $G1$ geometry, the $In_xGa_{1-x}N$ layer is more strained and for equivalent composition of indium and foil thickness $\Delta\epsilon_{xx}$ is higher. In the range of 3–20 nm the indium concentration can be expressed as in the case of $G1$ geometry: $x_{\mathrm{In}}=A_{G2}\Delta\epsilon_{xx}$. For example, for $t=7$ nm $A_{G1}=720$ and $A_{G2}=650$ which means that for the same measured distortion the In concentration will be higher in $G1$ geometry. The total InN content in the ternary layer, in units of InN monolayers inside QW, can be determined by integration of experimental maps of indium concentration $X_{\mathrm{In}}(x,z)$ along the x axis. And, if the criteria

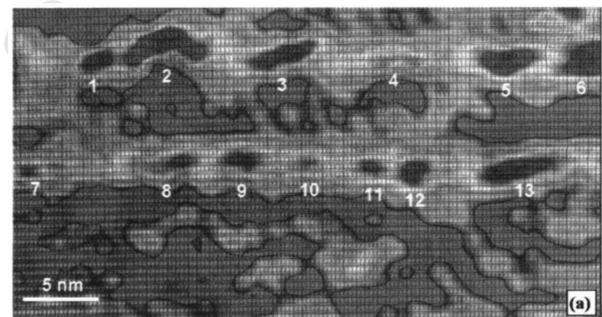

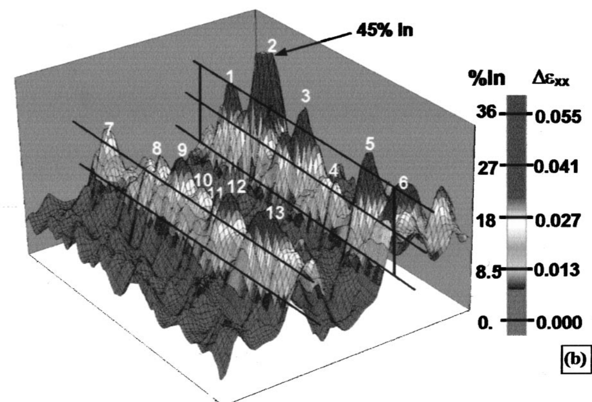

FIG. 5. Result of In composition evaluation inside the frame of Fig. 7. (a) Gray level coded In distribution superimposed on HRTEM image. Vertical and horizontal black lines show the grid used for composition evaluation. (b) Surface plot in perspective view. Numbers help for correspondence between (a) and (b).

PROOF COPY 006212JAP

PROOF COPY 006212JAP

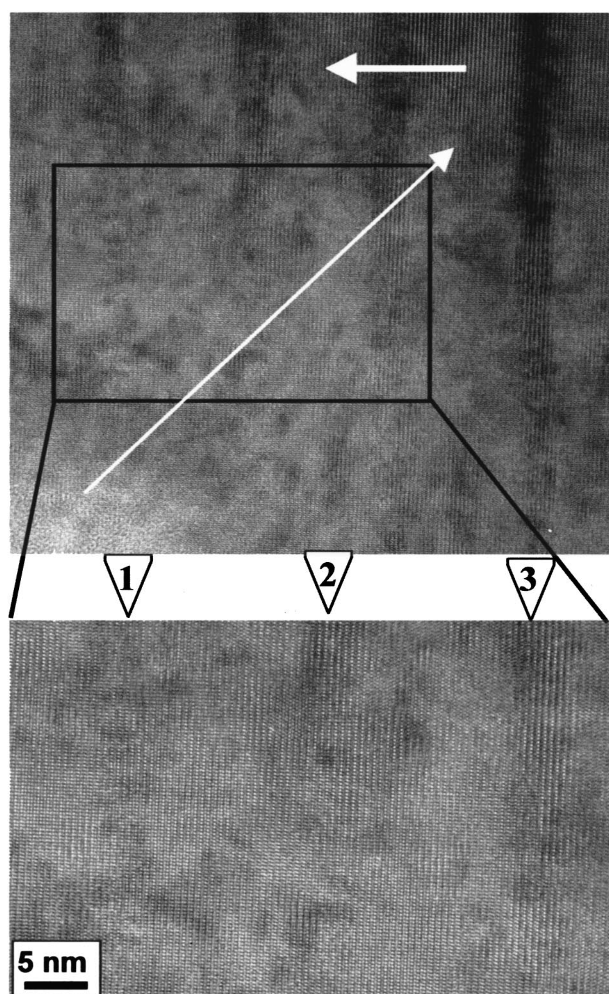

FIG. 6. HRTEM images of two InGaN (MBE) QWs along the $[11\bar{2}0]$ zone axis.

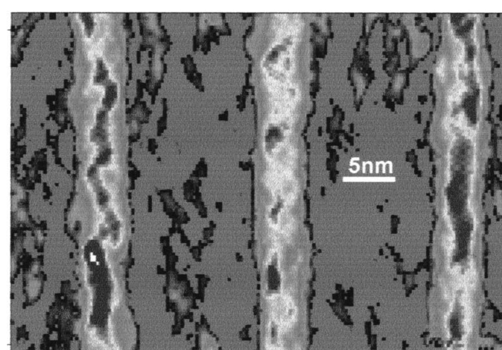

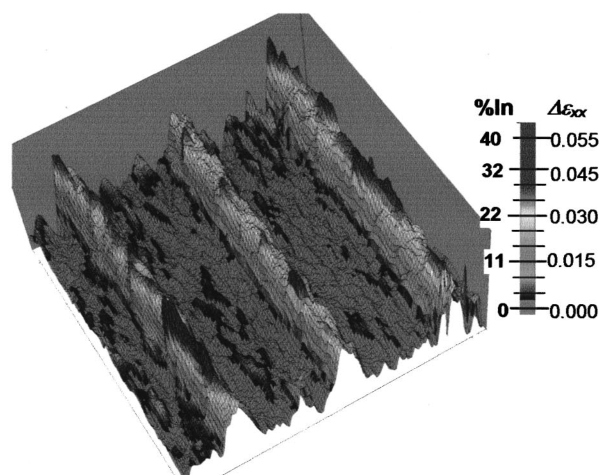

FIG. 7. (a) Strain map from the frame of Fig. 6 nonhomogeneous In distribution is clearly visible. (b) Surface plot in perspective view and calculated In composition.

for determination of QW thickness are set (for example, with at 20% of max In concentration) the average In concentration can be obtained $xa = X/W$ (W width of InGaN layer).

IV. EXPERIMENTAL RESULTS

A. MOCVD samples

A typical high-resolution image of a thin area used for composition evaluation is shown in Fig. 4. There are three QWs in this image. The whole image was processed, but only part of the area in the frame is suitable for quantitative evaluation. In this frame we have relatively slow rise of thickness for the two InGaN layers marked 1 and 2. In the neighborhood of the upper InGaN layer a large change in thickness is present, so it is not usable for quantitative evaluation. The strain distribution (Fig. 5) clearly shows maxima that can be attributed to indium reach clusters as suggested by Gerthsen *et al.*[13] As seen in Fig. 5(a), In segregation has a lateral size of about 2.5–3.5 nm and a height of about 2 nm. The thickness t of the zone shown in Fig. 4 is estimated to be between 5 and 10 nm, so the indium composition was calculated for a foil thickness $t = 7.5$ nm ($\mathbf{A} = 650$). This induces an error on the calculated indium concentration of $\pm 2.5\%$. Sometimes, clusters are very close to each other forming doublets or triplets in the image (projection) as can be seen for clusters 2, 3, 5, 8, 13. In the evaluated area, the foil thickness is larger than the size of clusters and the doublet image is due to superimposed isolated clusters. The maximum concentration of indium in cluster centers varies from 18 to 30. For the cluster marked 2, the measured In composition is 45%, in contrast, cluster 4 has a lower In concentration because it is probably not completely embedded in the foil [Fig. 5(b)].

B. MBE samples

High-resolution images obtained for the MBE sample have a more homogeneous contrast inside the InGaN QW in comparison to evaluated areas of MOCVD samples independently of the foil thickness (Fig. 6). The evaluated zone corresponds to the areas in the frame, its thickness is below 10 nm and no visible difference in mean contrast is observed between the InGaN layer and GaN spacer. For larger thickness, the position of InGaN layers starts to be clearly visible.

From composition evaluation, the In distribution is more homogeneous in comparison to the MOCVD analyzed sample (Fig. 7). Fluctuations of In are present, and the averaged peaks of concentration have higher values, 27.5% as compared to 24.1%, of the MOCVD sample. The peaks have more homogeneous values with smaller standard deviation

PROOF COPY 006212JAP

PROOF COPY 006212JAP

TABLE II. Statistics of the In concentration peaks in the uniform composition approximation.

	MOCVD	MBE
Average peak concent (% ln)	24.1	27.5
Standard dev. (% ln)	6.7	3.9
Max peak value (% ln)	44	40
Min peak value (% ln)	17	24
Average min between peaks (% ln)	13.6	22.2
Average amplitude of Δ ln conc min/max	0.56	0.81

3.9 (6.7 MOCVD). In the MOCVD sample, the concentration between peak drops to 13.6%, which is at least a half of maximal values (Table II).

The profiles obtained by vertical averaging of In distribution from Fig. 7 are different between the layers [Fig. 8(a)]. The maximum concentrations are, respectively, 27%, 23%, and 25%. The total In content obtained by integration of the profiles along the growth direction is, respectively, 1.85, 1.55, 1.85 equivalent monolayers of InN [Fig. 8(b)]. By taking 11c as the mean well width, the average In concentrations are: 16%, 13.5%, 16% for the three quantum wells, which is close to the nominal value of 15%.

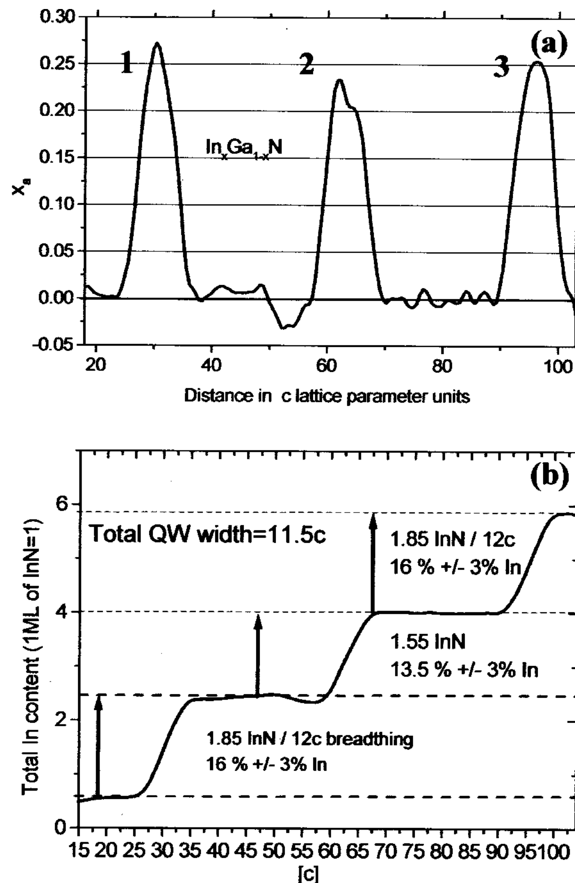

FIG. 8. (a) Profile of In concentration x obtained by vertical averaging of In distribution from Fig. 7(b). (b) Determination of total In content by integration of curve (a); the averaged indium concentration was calculated for 11.5 **c** wide QWs.

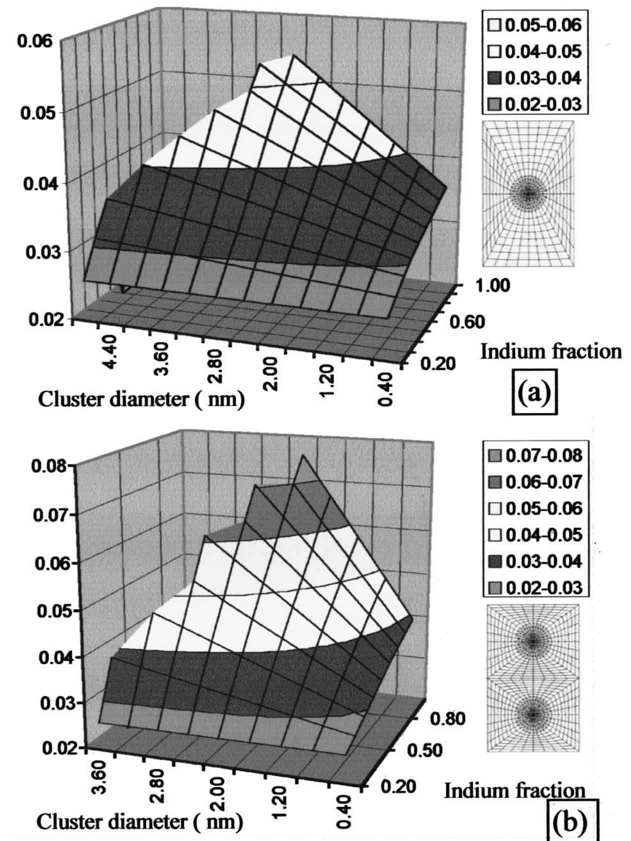

FIG. 9. (a) Calculated strain for one In rich cluster: nodes and geometry used for FE modeling of the cluster and average strain in function of the cluster diameter and composition. (b) Modeling of the MBE sample with two indium rich clusters: model geometry of the two In rich clusters and the average strain vs the cluster diameter and composition.

V. INDIUM CLUSTERING

The above discussion and interpretation of the composition of the layers has been carried out in the approximation of uniform In composition in the quantum wells. The measurements have demonstrated that this is not the case. Now one can look at the data in terms of clusters and try to determine the composition and size of each of them. As can be seen on the maps of the MOCVD quantum wells above, clusters are mainly separated and one can measure distances close to 5 nm between them. The size of each cluster appears to be 3 nm wide and 2 nm high. It is then possible to go back to the finite element modeling and take an average composition of 16% indium inside the three nm QWs. With the above geometry, it is probable to have only one cluster inside a 7-nm-thick foil, and we can locate it in the middle for the calculation of the projected strain profile. In Fig. 9(a) is shown the geometry (1 spherical cluster) for the calculation and the strain $\Delta\epsilon_{xx}$ in function of In composition and cluster diameter. As can be see, it will only be possible to measure $\Delta\epsilon_{xx}$ of 0.05 for a pure 2.8 nm InN cluster imbedded in a much lower indium matrix from the intended nominal 16% In QW.

In the case of the MBE quantum wells, the maximum value measured for $\Delta\epsilon_{xx}$ is also close to 0.05. However, the peaks of maximum deformation are rather close, and the size of the clusters seems to be in the range of 1.5 nm in height

PROOF COPY 006212JAP

PROOF COPY 006212JAP

and 2 nm in width. The average distance between them is about 3 nm. Using this input for a 7-nm-thick foil for TEM, it is possible to image two clusters in projection as seen in Fig. 9(b); the resulting $\Delta\epsilon_{xx}$ is 0.052 for two clusters of 1.6 nm diameter.

VI. DISCUSSION

The recent quantitative studies tended to show that indium composition fluctuation does occur independently of the growth method; of course most of the work has been carried out on MOCVD samples. In their report, Kisielowski and co-workers,[12] analyzed Nichia layers and demonstrated that indium rich clusters could be as small as 1–2 nm in lateral extension inside $In_{0.43}Ga_{0.67}N$ quantum wells. However, no typical In composition inside the clusters could be provided. In their strain analysis, Gerthsen *et al.*[13] also investigated MOCVD samples using lattice fringe HREM images recorded close to $[10\bar{1}0]$ zone axis. They determined the In composition within the thin/thick foil approximation and pointed out that the In may be present in clusters of 3-5 nm with concentration up to 70%–80% in layers of 10%–20% nominal composition.

Above, we have presented a comparative study of MOCVD and MBE InGaN quantum wells grown with similar nominal composition 15%–17%. Carrying out the observations along the $[11\bar{2}0]$ has allowed us to have smaller windows of sample thickness. The finite element modeling of the real sample geometry has shown that the measured strain can lead to determining the local composition within 2.5% accuracy. However, this analysis was carried out in the approximation of homogeneous In composition and peak compositions inside In clusters were found to be ~45% inside MOCVD and ~30% in MBE samples, respectively. By taking into account the clusters' average size, distance and TEM sample thickness, we then show that the homogeneous In composition model for the quantum wells leads to an underestimation of the cluster composition. In MOCVD samples, the strain comes from the projection of one indium rich cluster, whereas for MBE samples, there is a high probability that more than one cluster is always projected. The corresponding modeling of imbedded pure InN clusters leads to theoretical strains in agreement with the measured ones. It is, therefore, most probable that in both types of samples indium may segregate in the form of InN clusters that are 1–1.6 and 2–3 nm (height, width) in MBE and MOCVD, respectively.

VII. CONCLUSION

In summary, it has been possible to improve the accuracy of quantitative measurements of composition fluctuation inside InGaN ultrathin layers. It is pointed out that the main problem in HREM investigations is the projection of the data along the observation direction. Therefore, a reliable reconstruction of the three-dimensional configuration will need to use very thin sections (2–5 nm) and probably carry out observations along two zone axes ($[11\bar{2}0]$,$[10\bar{1}0]$). This will be possible using the procedure of chemical etching proposed earlier by Kisielowski and co-workers[12] in order to eliminate most of the amorphous surface layers on the TEM samples. For such investigations, three beam images, which mask the effects of thickness fluctuation and allow the use of thicker areas, are not a good way for monitoring the evaluated areas, nor for separating individual clusters. In this investigation, it is clearly shown that both growth methods lead to the formation of In rich clusters, which are smaller in MBE, layers.

ACKNOWLEDGMENTS

This work is supported by the EU under Contract No. HPRN-CT-1999-00040 and the MENRT under "Action Incitative Nanotechnologie: Boquani." Part of the FE calculations have been supported by the State Committee for Scientific Research (KBN) under Grant No. 7 T07A 004 16. M.A. di Forte Poisson from Thales Group, N. Grandjean, J. Massies and B. Damilano from CRHEA are gratefully acknowledged for their continuous interest in the authors' work and for providing them with the InGaN layers.

[1] S. Nakamura and G. Fazol, *The Blue Laser Diode* (Springer, Berlin, 1997).
[2] Y. Narukawa, Y. Kawakami, M. Funato, S. Fujita, S. Fujita, and S. Nakamura, Appl. Phys. Lett. **70**, 681 (1997).
[3] I. Ho and G. B. Stringhellow, Appl. Phys. Lett. **69**, 2201 (1996).
[4] R. Singh, D. Dappalapudi, T. D. Maussakas, and L. T. Romano, Appl. Phys. Lett. **70**, 1089 (1997).
[5] M. D. Mceluskey, L. T. Romano, B. S. Krusar, D. P. Baur, and W. M. Johsan, Appl. Phys. Lett. **72**, 1730 (1998).
[6] S. F. Chichilu, K. Wada, J. Miillhäuser, O. Brandt, K. H. Ploog, T. Mizutani, A. Setoguchi, Rnakai, M. Sugigama, H. Nakamichi, K. Kori, T. Deguchi, T. Sota, and S. Nakamura, Appl. Phys. Lett. **76**, 1971 (2000).
[7] H. C. Yang, P. F. Kuo, Y. Y. Lin, Y. F. Chen, K. H. Chen, L. C. Chen, and J. I. Chyi, Appl. Phys. Lett. **76**, 3712 (2000).
[8] H. O. O'Donnell, R. W. Martin, and G. P. Middleton, Phys. Rev. Lett. **82**, 237 (1999).
[9] P. Ruterana, G. Nouet, W. Van der Stricht, I. Moerman, and L. Considine, Appl. Phys. Lett. **72**, 1742 (1998).
[10] D. Doppalapudi, S. N. Basu, and T. D. Moustakas, J. Appl. Phys. **85**, 883 (1999).
[11] M. K. Behbehani, E. L. Piner, S. X. Liu, N. A. El-Masry, and S. M. Bedair, ■, **75**, 2202 (1999).
[12] C. Kisielowski, Z. Liliental Weber, and S. Nakamura, Jpn. J. Appl. Phys., Part 1 **36**, 6932 (1997).
[13] D. Gerthsen, E. Hahn, B. Neubauer, A. Rosenauer, O. Schön, M. Heuken, and A. Rizzi, Phys. Status Solidi A **177**, 145 (2000).
[14] N. G. Chew and A. G. Cullis, Ultramicroscopy **23**, 175 (1987).
[15] R. W. Glaisher, A. E. C. Spargo, and D. J. Smith, Ultramicroscopy **27**, 117 (1989).
[16] *Optimas 6.5 User Guide and Technical Reference* (Media Cybernetics, 1999).
[17] A. Rosenauer, T. Remmele, D. Gerthsen, K. Ullmann, and A. Foster, Optik (Stuttgart) **105**, 99 (1997).
[18] S. Kret, P. Ruterana, A. Rosenauer, and D. Gerthsen, Phys. Status Solidi **227**, 247 (2001).
[19] M. M. J. Treacy and J. M. Gibson, J. Vac. Sci. Technol. B **4**, 1458 (1986).
[20] K. Tillmann, M. Lentzen, and R. Rosenfeld, Ultramicroscopy **83**, 111 (2000).
[21] O. C. Zienkiewicz and R. J. Taylor, *The Finite Element Method*, 4th ed. (McGraw–Hill, London, 1989).
[22] M. A. Crisfield, *Non-Linear Finite Element Analysis of Solid and Structures* (Wiley, New York, 1997).
[23] P. Dłużewski and G. Maciejewski, Int. J. Plasticity (submitted).
[24] J. E. Sinclair, P. C. Gehlen, R. G. Hoagland, and J. P. Hirth, J. Appl. Phys. **49**, 3890 (1978).
[25] P. Dłużewski, J. Elast. **60**, 119 (2000).
[26] R. R. Reeber and K. Wang, MRS Internet J. Nitride Semicond. Res. **6**, 3 (2001).

PROOF COPY 006212JAP